Hesperadin sensitizes gastric cancer cells to cisplatin via NOX1-dependent oxidative stress

WANJING ZHU[1], QIYIN LI[1], ZHENGLEI JI[2], DI WU[1], JINGYA CHEN[2], YUNLI ZHAO[2] and HUAZHANG WU[1]

[1]School of Life Science, Anhui Provincial Key Laboratory of Tumor Evolution and Intelligent Diagnosis and Treatment, Bengbu Medical University, Bengbu, Anhui 233030, P.R. China; [2]School of Public Health, Bengbu Medical University, Bengbu, Anhui 233030, P.R. China

Received July 10, 2025; Accepted September 30, 2025

DOI: 10.3892/br.2025.2076

Abstract. The therapeutic efficacy of cisplatin in gastric cancer (GC) is frequently constrained by chemoresistance and systemic toxicity. Targeted small molecules hold promise for providing synergistic effects that enhance treatment outcomes. GC cell viability was assessed via a Cell Counting Kit-8 (CCK-8) assay. Apoptosis, intracellular reactive oxygen species (ROS) levels, and the mitochondrial membrane potential were evaluated via flow cytometry and JC-1 staining. Transcriptomic analysis [RNA-sequencing (RNA-Seq)] was subsequently conducted to identify differentially regulated pathways, followed by validation via reverse transcription-quantitative PCR and western blotting. DNA damage was measured by γ-H2AX immunofluorescence, and clonogenic survival was examined. The NOX1-specific inhibitor ML171 was used to verify its mechanistic involvement. Hesperadin markedly suppressed GC cell proliferation in a dose-dependent manner and induced mitochondrial apoptosis by regulating the Bcl-2/Bax ratio and activating caspase pathways. RNA-Seq analysis revealed significant upregulation of NOX1 and activation of oxidative stress-associated pathways following Hesperadin treatment. Cotreatment with Hesperadin and cisplatin markedly reduced the IC_{50} of cisplatin, increased ROS accumulation, aggravated DNA damage, and potentiated apoptotic cell death. Notably, ML171 attenuated ROS generation and apoptotic effects, confirming the occurrence of a NOX1-dependent mechanism. In conclusion, Hesperadin enhances the sensitivity of GC cells to cisplatin by inducing NOX1-mediated oxidative stress and promoting mitochondrial dysfunction-driven apoptosis, underscoring its potential as an effective combinatorial therapeutic strategy for GC treatment.

Correspondence to: Professor Yunli Zhao, School of Public Health, Bengbu Medical University, 2600 Donghai Avenue, Bengbu, Anhui 233030, P.R. China
E-mail: yunli@126.com

Professor Huazhang Wu, School of Life Science, Anhui Provincial Key Laboratory of Tumor Evolution and Intelligent Diagnosis and Treatment, Bengbu Medical University, 2600 Donghai Avenue, Bengbu, Anhui 233030, P.R. China
E-mail: wuhuazhang@bbmu.edu.cn

Key words: hesperadin, NOX1, oxidative stress, apoptosis, chemo-sensitization

Introduction

Gastric cancer (GC) is a highly prevalent malignant tumor worldwide. According to GLOBOCAN 2022 data released by the International Agency for Research on Cancer, the incidence and mortality rates of GC rank fifth among all malignant neoplasms globally, with an estimated 970,000 new cases and 660,000 deaths annually (1). Because most patients are diagnosed at advanced or metastatic stages, thereby forfeiting the opportunity for curative surgical intervention, there is an urgent need to develop more effective and less toxic chemotherapeutic agents for GC management (2,3).

Cisplatin, a first-line chemotherapeutic agent, plays a crucial role in treating GC by inducing DNA cross-linking damage and generating reactive oxygen species (ROS) (4,5). However, its clinical application is often associated with pronounced nephrotoxicity and neurotoxicity, which substantially constrain its prolonged use and optimal dosing (6-8). In recent years, the combination of small-molecule compounds with cisplatin has attracted considerable attention because of their synergistic and toxicity-reducing properties. This approach can lower the required dose of cisplatin while enhancing tumor cell sensitivity to chemotherapy (9-11). Therefore, identifying small-molecule compounds capable of eliciting synergistic effects at low concentrations represents a promising approach to enhancing cisplatin-based therapeutic regimens in patients with GC. Hesperadin is a small-molecule kinase inhibitor identified through high-throughput screening (12-14). It has been demonstrated that Hesperadin possesses dual functions: Antitumor and cardioprotective properties. First, by targeting and inhibiting Aurora B kinase, which regulates mitosis and mediates antitumor activity, as well as calcium/calmodulin-dependent protein kinase II-δ (CaMKII-δ), which is involved in the oxidative stress response, Hesperadin has exhibited significant antiproliferative and proapoptotic effects in various tumor models. Second, the inhibition of CaMKII-δ can mitigate the damage caused by chemotherapeutic drugs to cardiac tissues (15). These properties, along with their ability to reduce toxicity, offer unique advantages for clinical application. Hesperadin

exerts its antitumor activity through dual inhibition of Aurora B and CaMKII-δ kinases, and its remarkable potency is reflected in its exceptionally low IC_{50}values. Consistent with a previous study in pancreatic cancer (16), the present findings demonstrated that Hesperadin exhibits potent antitumor effects at nanomolar concentrations in GC cells.

The dual functional properties of Hesperadin offer a novel therapeutic avenue for combination chemotherapy. By targeting and modulating downstream molecular activities, Hesperadin increases tumor cell sensitivity to chemotherapeutic agents while simultaneously mitigating treatment-associated toxicity. However, its specific role in GC and its potential synergistic interactions with cisplatin remain incompletely understood. In the present study, it was demonstrated that hesperadin induces NOX1-dependent ROS generation, thereby increasing the sensitivity of GC cells to cisplatin. These findings not only establish a connection between Hesperadin and the efficacy of cisplatin but also suggest new possibilities for combination chemotherapy regimens in the treatment of advanced GC.

Materials and methods

Cell culture. The human GC cell lines AGS and HGC-27 were procured from the Cell Resource Center of the Chinese Academy of Medical Sciences in collaboration with Peking Union Medical College. The cells were cultured in Dulbecco's Modified Eagle's Medium (DMEM; Gibco; Thermo Fisher Scientific, Inc.) supplemented with 10% heat-inactivated fetal bovine serum (FBS; Wisent, Inc.). The cells were maintained at 37˚C in a humidified incubator with 5% CO_2 (Thermo Fisher Scientific, Inc.).

Drugs and reagents. Hesperadin (cat. no. HY-12054; MedChemExpress) and cisplatin (cat. no. 232120; MilliporeSigma) were dissolved in dimethyl sulfoxide (DMSO) and normal saline, respectively, and stored at -20˚C in light-protected conditions. The NOX1 inhibitor ML171 (2-acetylphenothiazine; cat. no. HY-12805; MedChemExpress) was also dissolved in DMSO before use. The Cell Counting Kit-8 (CCK-8; cat. no. C0038), Annexin V-FITC apoptosis detection kit (cat. no. C1062M), ROS detection kit (cat. no. S0033S), JC-1 mitochondrial membrane potential (MMP; cat. no. C2006) assay kit and DNA damage detection kit (cat. no. C2035S) were obtained from Beyotime Institute of Biotechnology.

Cell proliferation and cytotoxicity assays. To evaluate cytotoxicity, AGS and HGC-27 GC cells were seeded in 96-well plates at a density of 6,000 cells per well and exposed to Hesperadin (0-90 nM) or cisplatin (0-120 μM) for 24 h. After 48 h of treatment, CCK-8 reagent (10 μl per well) was added and incubated at 37˚C for 2 h. The absorbance at 450 nm was then measured using a SpectraMax iD5 microplate reader (Molecular Devices, LLC) to determine the half-maximal inhibitory concentration (IC_{50}) values using statistical software.

For the proliferation inhibition assay, cells were seeded at the same density and treated with Hesperadin alone or in combination with cisplatin for 48 h. The procedures for CCK-8 reagent incubation and absorbance measurement at 450 nm were performed as described for the cytotoxicity assay.

RNA sequencing (RNA-seq) and bioinformatics. RNA extraction, library preparation, and sequencing were performed by Shanghai Applied Protein Technology Co., Ltd. Briefly, total RNA was extracted from AGS cells using TRIzol® Reagent (cat. no. R0016; Beyotime Institute of Biotechnology). RNA integrity was verified (RIN >8.0). Sequencing libraries were constructed using the VAHTS Universal V6 RNA-seq Library Prep Kit for Illumina (Vazyme Biotech Co., Ltd.) and sequenced on an Illumina NovaSeq 6000 platform to generate 150 bp paired-end reads. Subsequent bioinformatic analysis was conducted as follows: Raw reads were quality-filtered using Fastp. *De novo* assembly was performed with Trinity. Transcripts were annotated against NR (https://www.ncbi.nlm.nih.gov/refseq/about/nonredundantproteins/), SwissProt (https://www.uniprot.org/uniprotkb?facets=reviewed%3Atrue), Pfam (http://pfam.xfam.org/), Gene Ontology (GO; http://geneontology.org/) and Kyoto Encyclopedia of Genes and Genomes (KEGG; https://www.genome.jp/kegg/) databases. Coding sequences were predicted using TransDecoder. Gene expression (FPKM) was quantified, and differential expression analysis was performed using DESeq2 (threshold: |log2FC|>1, padj <0.05). GO and KEGG enrichment analyses were conducted using clusterProfiler (version 4.16.0; Bioconductor).

Identification of differentially expressed genes (DEGs) and functional enrichment analysis. With |log2-fold change (FC)|>1 and P<0.05 as screening criteria, DEGs from bulk sequencing were identified via the 'Limma' package (version 3.64.3; Bioconductor) of R. DEGs were illustrated via volcano maps and heatmaps, which were plotted via the 'ggplot2' and 'Pheatmap' packages of R, respectively. In addition, KEGG and GO analyses were performed via the 'clusterProfiler' R package, which aims to assess gene-related biological processes (BP), molecular functions, cellular components, and gene-related signaling pathways (KEGG). The conditions for screening significantly enriched GO terms and KEGG pathways were Min overlap=three and Min enrichment=1.5. The enrichment significance threshold was set to an adjusted P-value below 0.05. In addition, gene set variation analysis (GSVA) is a non-parametric and unsupervised method for estimating changes in specific gene sets. The activities of the hallmark pathways were quantified with the GSVA R package according to the 'Hallmarks geneset' downloaded from the MsigDB database. Finally, gene set enrichment analysis (GSEA) was employed to identify DEG functions on the basis of P<0.05 and a false discovery rate (FDR) value of 0.25.

Flow cytometric analysis of apoptosis and necrosis. Apoptosis was assessed using an Annexin V-FITC/propidium iodide (PI) apoptosis detection kit (cat. no. C1062M; Beyotime Institute of Biotechnology). Briefly, after drug treatment, the cells were collected, washed twice with ice-cold PBS, and resuspended in 1X binding buffer at a density of $1x10^6$ cells/ml. Subsequently, cells were stained with Annexin V-FITC and PI for 15 min at room temperature in the dark according to the manufacturer's instructions. To establish appropriate gating and compensation, unstained cells and single-stained controls (cells stained with Annexin V-FITC only or PI only) were included in each experiment. Flow cytometric analysis was immediately performed on

a Beckman CytoFLEX flow cytometer (Beckman Coulter, Inc.). The data were analyzed using FlowJo software (version 10.8.1; FlowJo LLC). The percentages of cells in early apoptosis (Annexin V^+/PI^-) and late apoptosis/necrosis (Annexin V^+/PI^+) were quantified.

Detection of intracellular ROS levels. For ROS detection, following the respective treatments, cells were collected, washed twice with pre-warmed phosphate-buffered saline (PBS), and then incubated with 10 μM CM-H2DCFDA diluted in serum-free medium at 37˚C in the dark for 25 min. After incubation, the cells were washed to remove the excess probe and analyzed using a fluorescence microscope (MShot MF53-N, FITC channel), and the captured images were quantified using ImageJ software (version 1.53k; National Institutes of Health). The fluorescence intensity was quantified via flow cytometry (FITC channel).

MMP assay. The MMP was assessed via a JC-1 assay kit (cat. no. C2006; Beyotime Institute of Biotechnology). The cells were incubated with JC-1 staining solution for 20 min at 37˚C in the dark for 20 min. The fluorescence intensity ratios (red/green) were subsequently analyzed via fluorescence microscopy (MShot MF53-N). JC-1 aggregates (red fluorescence) in healthy mitochondria with high MMP and JC-1 monomers (green fluorescence) in depolarized mitochondria with low MMP were detected using the TRITC and FITC channels, respectively. For quantitative analysis, the fluorescence intensity of the red and green channels from the captured images was measured using ImageJ software (version 1.53k; National Institutes of Health).

DNA damage assay. The cells were fixed for 15 min and subsequently incubated overnight at 4˚C with the γ-H2AX primary antibody (cat. no. C2035S; Beyotime Institute of Biotechnology). After three gentle rinses with phosphate-buffered saline (PBS), the cells were incubated for 1 h with an Alexa Fluor 488-conjugated goat anti-rabbit secondary antibody. Nuclei were counterstained with DAPI (10 μg/ml) for 5 min. Fluorescence images were captured via a fluorescence microscope (MShot MF53-N). The number of γ-H2AX foci per cell was quantified via the 'Analyze Particles' function in ImageJ software (version 1.53k).

RNA extraction and reverse transcription-quantitative PCR (RT-qPCR) analysis. Total RNA was extracted from cultured AGS and HGC-27 cells using an RNA extraction kit (Omega Bio-Tek, Inc.). cDNA was synthesized from 1 μg RNA using the SweScript RT SuperMix (Wuhan Servicebio Technology Co., Ltd.). with the following thermal protocol: 25˚C for 5 min, 42˚C for 15-30 min, and 85˚C for 5 sec. qPCR was performed on a QuantStudio 5 system (Applied Biosystems; Thermo Fisher Scientific, Inc.) using Servicebio SYBR Green Master Mix. The thermocycling protocol was as follows: 95˚C for 10 min; 40 cycles of 95˚C for 15 sec and 60˚C for 1 min. The relative expression of NOX1 was normalized to GAPDH and calculated using the $2^{-\Delta\Delta Cq}$ method (17). The sequences of primers used were as follows: NOX1 forward, 5'-TCTGGTTGTTTGGTTAGG GCT-3' and reverse, 5'-CGGCTGCAAAACCCAAGGA-3'; and GAPDH forward, 5'-CGGAGTCAACGGATTTGG TCGTAT-3' and reverse, 5'-AGCCTTCTCCATGGTGGT GAAGAC-3'.

Colony formation assay. The GC cell lines were seeded into culture plates. After adhering, the cells were treated with the designated concentrations for 10 days, followed by staining with 0.1% crystal violet for 30 min. The plates were rinsed with ultrapure water, air-dried, and scanned. Colonies containing more than 50 cells were automatically quantified using ImageJ software (version 1.53k; National Institutes of Health).

Western blot analysis. Cells were lysed in RIPA buffer (cat. no. P0013B; Beyotime Institute of Biotechnology) supplemented with 1% PMSF. The protein concentration was determined using a BCA Protein Assay Kit (cat. no. P0010; Beyotime Institute of Biotechnology). In total, ~20-30 μg of total protein per lane was separated on 12.5% SDS-PAGE gels (Epizyme, Inc.) and transferred onto polyvinylidene fluoride (PVDF) membranes (MilliporeSigma). The membranes were blocked with 5% non-fat milk in TBST (0.1% Tween-20) for 2 h at room temperature and then incubated overnight at 4˚C with the following primary antibodies: anti-BCL-2 (1:2,000; cat. no. 12789-1-AP; Proteintech Group, Inc.), anti-BAX (1:20,000; cat. no. 50599-2-Ig; Proteintech Group, Inc.), anti-caspase-3/cleaved caspase-3 (1:1,000; cat. no. 19677-1-AP; Proteintech Group, Inc.), anti-NOX1 (1:1,000; cat. no. 671300; Chengdu Zhengneng Biotechnology, Co., Ltd.), anti-β-ACTIN (1:50,000; cat. no. 66009-1-Ig; Proteintech Group, Inc.) and anti-GAPDH (1:20,000; cat. no. 10494-1-AP; Proteintech Group, Inc.). After washing, the membranes were incubated with HRP-conjugated Goat Anti-Rabbit IgG (1:5,000; cat. no. SA00001-2; Proteintech Group, Inc.) or HRP-conjugated Goat Anti-Mouse IgG (1:5,000; cat. no. SA00001-1; Proteintech Group, Inc.) secondary antibodies for 1 h at room temperature. Protein bands were visualized using an Enhanced Chemiluminescence (ECL) Substrate (cat. no. WBKLS0500; MilliporeSigma) and captured digitally. The band intensities were quantified by densitometry using ImageJ software (version 1.53k; National Institutes of Health).

Small interfering RNA (siRNA) transfection. For siRNA transfection, cells were cultured in 6-well plates until they reached ~70-90% confluence. Specific siRNAs were then transfected via Lipofectamine 2000 reagent (cat. no. 11668-027; Thermo Fisher Scientific, Inc.). A final concentration of 20 μM of siRNA was used for each transfection. The transfection was carried out in serum-free Opti-MEM medium and incubated with the cells at 37˚C for 4 h, after which the medium was replaced with complete growth medium. The efficiency of siRNA-mediated interference was verified 48 h post-transfection via western blotting to ensure effective knockdown of the target genes. All siRNAs, including the non-targeting negative control (si-NC), were designed and synthesized by Anhui General Biotech Co., Ltd. The siRNA sequences utilized in the present study were as follows: siNOX1#1 (homo-ID27035 siRNA-318) forward, 5'-AUGAGAAGG CCGACAAAUATT-3' and reverse, 5'-AUUUGCGCAGGC UCUUUGCTT-3'; siNOX1#2 (homo-ID27035 siRNA-1315) forward, 5'-CAUAAGGGCUUUCGAACAATT-3' and

reverse, 5'-UUGUUCGAAAGCCCUUAUGTT-3'; and si-NC forward, 5'-UUCUCCGAACGUGUCACGUTT-3' and reverse, 5'-ACGUGACACGUUCGGAGAATT-3'.

Statistical analysis. The data are presented as the mean ± SDs of three independent biological replicates. Statistical comparisons between two groups were performed using an unpaired Student's t test. For comparisons among more than two groups, one-way analysis of variance (ANOVA) was employed, followed by Tukey's post hoc test. $P<0.05$ was considered to indicate a statistically significant difference. All statistical analyses were performed via GraphPad Prism software (version 9.5.1; Dotmatics).

Results

Hesperadin induces cell death and inhibits proliferation in GC cells. To assess the antitumor activity of Hesperadin, its IC50 in GC cell lines was first determined. The IC50 values of Hesperadin in AGS and HGC-27 cells were 52.49 nM and 46.37 nM, respectively (Fig. 1A). Next, concentrations of 10 and 20 nM were selected for AGS cells and 8 and 16 nM for HGC-27 cells, all of which are below the IC50 values for subsequent experiments. Compared with the control, Hesperadin significantly inhibited the proliferation of GC cells in a concentration-dependent manner (Fig. 1B).

To further examine the growth-inhibitory effects of Hesperadin on GC cells, Annexin V-FITC/PI double staining followed by flow cytometry was performed to evaluate its effect on cell death. Flow cytometry revealed increased cell death after 48 h of treatment (Fig. 1C). Western blot analysis demonstrated that hesperadin significantly downregulated the expression of the antiapoptotic protein BCL-2 while upregulating the expression of the proapoptotic proteins BAX and cleaved caspase-3. These findings indicated that Hesperadin promotes cell death through activation of the mitochondrial apoptosis pathway (Fig. 1D). Taken together, these results demonstrated that Hesperadin suppresses GC cell proliferation and induces cell death in a dose-dependent manner via activating the mitochondrial apoptosis pathway.

Transcriptomic analysis suggests that Hesperadin may induce GC cell death through the apoptosis and oxidative stress pathways. Inducing the apoptosis of tumor cells is one of the important ways to inhibit cell proliferation (18). To elucidate the molecular mechanisms driving Hesperadin-induced cell death in GC, RNA-seq was conducted on AGS cells treated with 10 nM Hesperadin for 48 h. A complete list of all DEGs is provided in Table SII. The DEGs identified from the RNA-seq results are illustrated in Fig. 2A and B. GO, KEGG, GSEA and GSVA enrichment analyses revealed that the DEGs were significantly enriched in BP such as apoptosis and the oxidative stress response (Fig. 2C-F). While the top 10 upregulated DEGs were associated with key cancer pathways such as cell cycle arrest (for example, CDKN1A), p53 signaling (for example, BTG2) and cell adhesion (for example, PTPRU) (Table SI), the pronounced enrichment in oxidative stress pathways particularly captured our attention. Specifically, GO analysis identified significant enrichment in the 'cellular response to oxidative stress' (GO: 0045489) (Fig. 2C) and KEGG analysis confirmed enrichment in the 'Oxidative phosphorylation' pathway (hsa00190) (Fig. 2D). This transcriptional profile aligns with the documented mechanism of Hesperadin, which induces mitochondrial dysfunction and a ROS surge in other cancer models (16). Consequently, DEGs within these oxidative stress-related pathways were prioritized for further investigation. Among them, NADPH Oxidase 1 (NOX1) emerged as a compelling candidate. Although its fold-change ranked outside the top 10, NOX1 encodes a critical catalytic subunit of the NADPH oxidase complex, a dedicated superoxide generator and a master regulator of oxidative stress (19,20). Its significant upregulation ($\log_2$FC >1.5, $P<0.01$) following Hesperadin treatment (Fig. 2A) suggested a functionally central role in mediating the observed oxidative stress phenotype. NOX1 was therefore selected for subsequent functional validation.

Hesperadin promotes GC cell death by activating the oxidative stress pathway through the induction of ROS generation. Excessive production of ROS induces oxidative stress and mitochondrial dysfunction, ultimately leading to cell death (18,19). To investigate the impact of Hesperadin on ROS generation and oxidative stress pathways in GC cells, intracellular ROS levels in AGS and HGC-27 cells were measured following Hesperadin treatment. The results showed a significant, concentration-dependent increase in ROS fluorescence intensity in the Hesperadin-treated cells compared with the control group (Fig. 3A). Further quantitative analysis by flow cytometry revealed that Hesperadin increased ROS levels in GC cells in a dose-dependent manner (Fig. 3B). In summary, it can be concluded that Hesperadin induces cell death in GCs by increasing the generation of ROS, which leads to oxidative stress and activates the mitochondrial apoptotic pathway.

Hesperadin increases the sensitivity of GC cells to cisplatin. Cisplatin is a key chemotherapeutic agent widely used in the treatment of GC (21,22). Considering the mechanistic similarities between cisplatin and Hesperadin in modulating tumor-associated pathways, the present study aimed to evaluate the potential therapeutic benefits of combining both agents in GC cell models. To investigate the potential combinatorial effect of Hesperadin and cisplatin, the IC_{50} for each agent alone was first determined in AGS and HGC-27 cells (Figs. 1A and 4A). To distinguish true synergy from additive toxicity, sub-IC_{50} concentrations were selected for all combination treatments. Based on dose-response profiles and preliminary validation, the chosen concentrations (20 nM Hesperadin and 10 μM cisplatin for AGS cells, and 16 nM Hesperadin and 8 μM cisplatin for HGC-27 cells) represent ~30-40% of their respective single-agent IC_{50} values. These doses induce partial biological effects (Fig. 1B and C) and moderate proliferation inhibition without causing overwhelming cell death, thereby providing a clear window to observe enhanced efficacy upon combination. Under these conditions, the combinatorial effects were evaluated. The results revealed that when AGS and HGC-27 cells were treated with a combination of Hesperadin and cisplatin, the IC_{50} values for cisplatin decreased from 33.66 and 26.88 μM to 24.99 and 20.47 μM, respectively (Fig. 4A). Furthermore, the GC cell survival rate in the Hesperadin-cisplatin combination

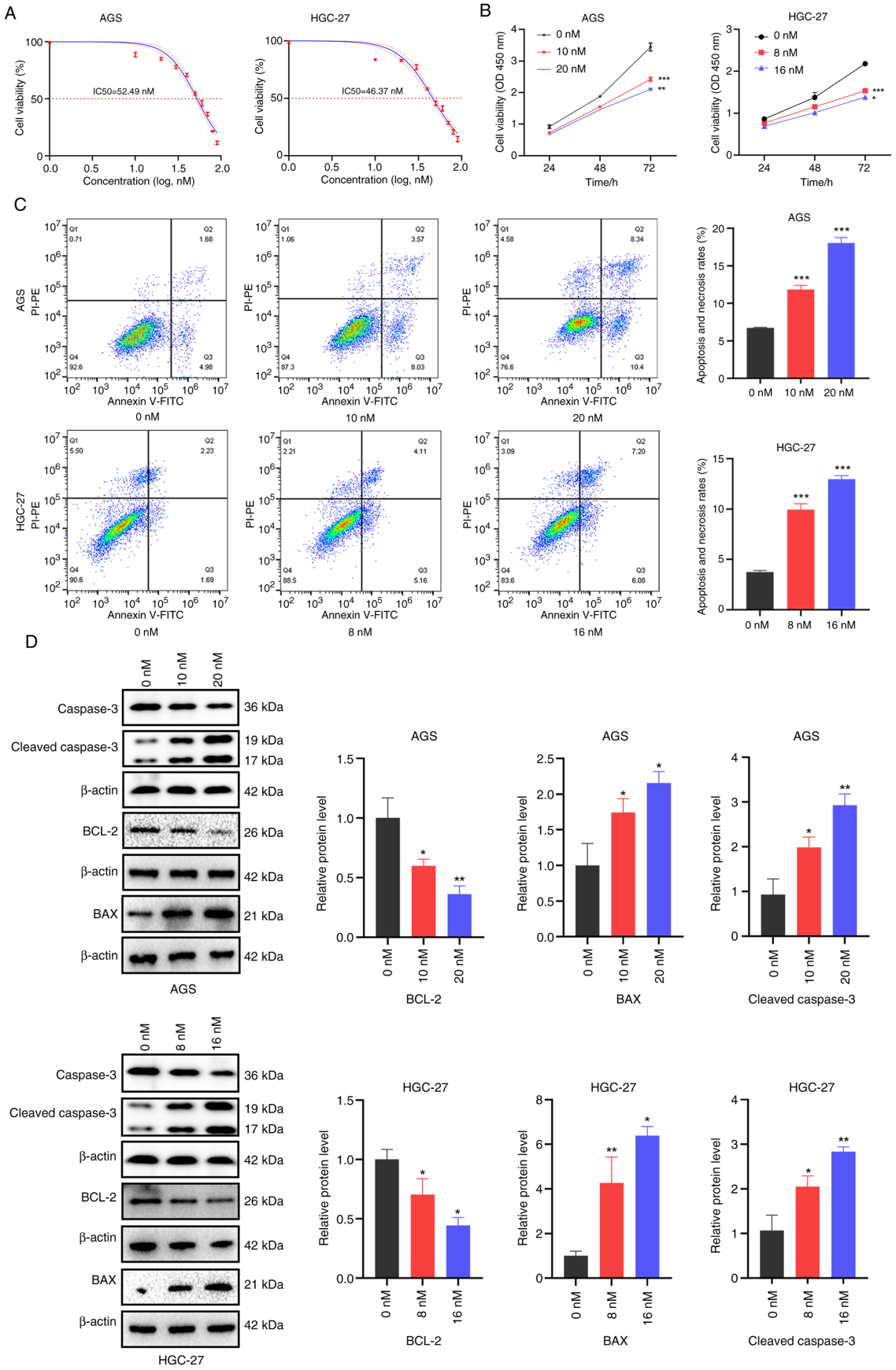

Figure 1. Hesperadin inhibits proliferation and induces death in gastric cancer cells. (A) After the cells were treated with graded concentrations of hesperadin (0, 10, 20, 30, 40, 50, 60, 70, 80 and 90 nM) for 48 h, cell viability was assessed via the CCK-8 assay, and the IC_{50} was calculated. (B) A CCK-8 assay was used to evaluate the viability of AGS and HGC-27 cells following 24, 48 and 72 h of Hesperadin treatment. (C) Flow cytometric analysis was conducted to assess cell mortality after 48 h of Hesperadin treatment. (D) The expression levels of the apoptosis-related proteins BCL-2, BAX and cleaved caspase-3 were analyzed via western blotting. β-ACTIN was used as a loading control. Compared with the control group, the high-concentration group was compared with the low-concentration group; *P<0.05, **P<0.01 and ***P<0.001. CCK-8, Cell Counting Kit.

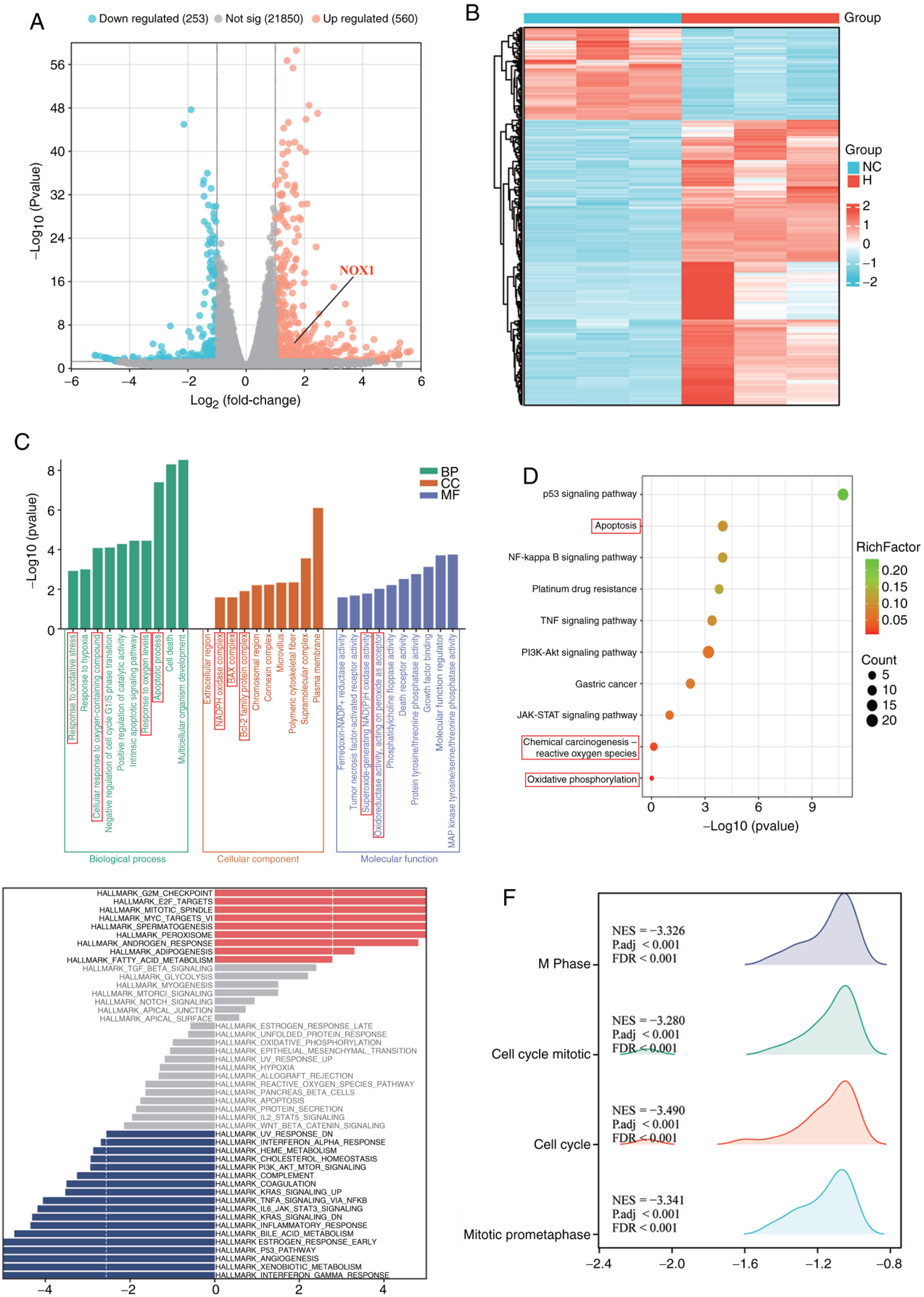

Figure 2. Transcriptomic analysis of Hesperadin-induced model cell lines. (A) Volcano plot showing the DEGs. (B) Heatmap illustration of significant DEGs. (C) Gene Ontology enrichment analysis of DEGs. (D) Kyoto Encyclopedia of Genes and Genomes pathway enrichment analysis of DEGs. (E) GSEA of DEGs. (F) GSVA enrichment analysis. DEGs, differentially expressed genes; GSEA, gene set enrichment analysis; GSVA, gene set variation analysis; FDR, false discovery rate.

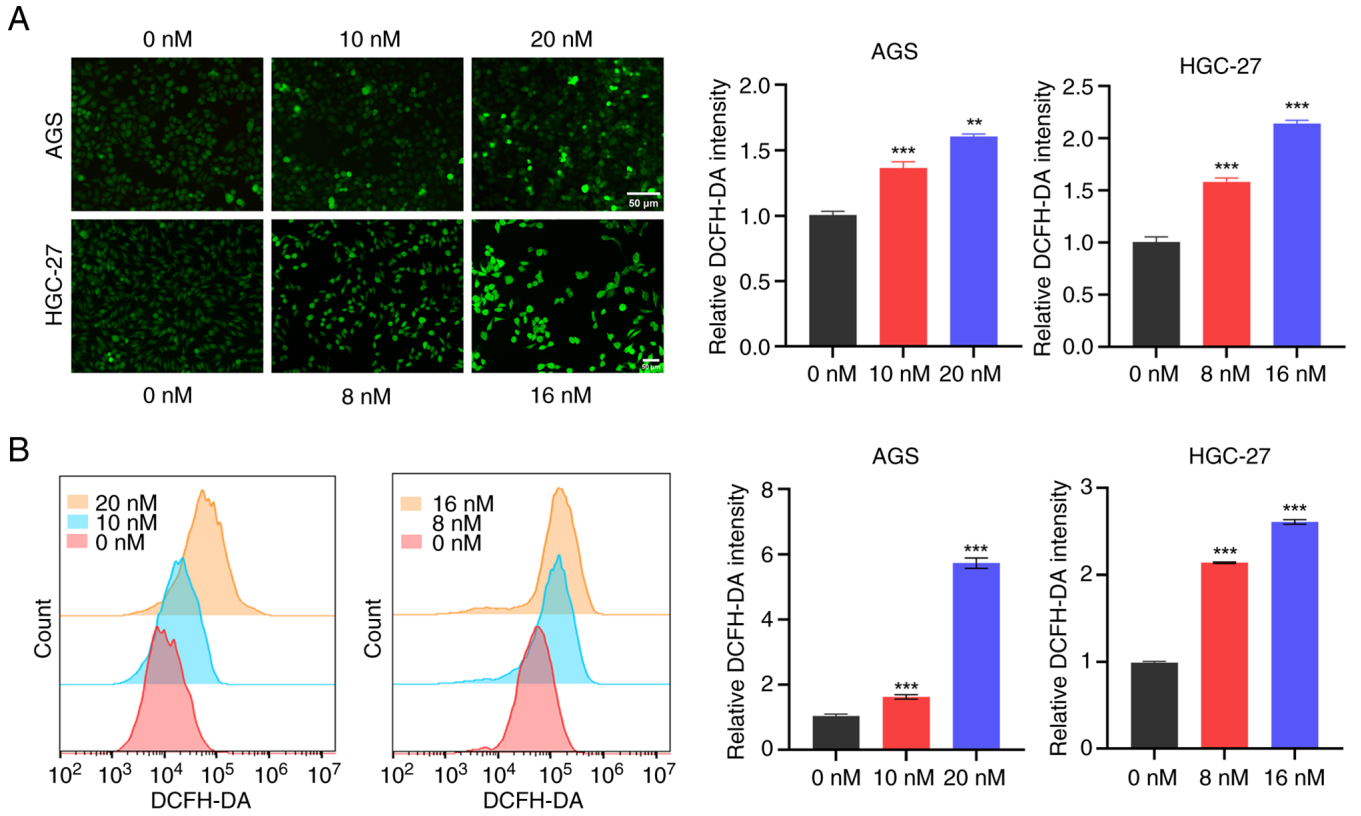

Figure 3. Hesperadin induces cell death in GC cells by activating oxidative stress via ROS generation. (A) DCFH-DA fluorescence staining was utilized to measure the production of ROS in GC cells following Hesperadin treatment (green fluorescence indicates ROS; scale bar, 50 μm). (B) Flow cytometry was used to quantify the ROS levels (shown as the mean DCF fluorescence intensity) in the groups treated with Hesperadin. Compared with the control group, the high-concentration group was compared with the low-concentration group; **P<0.01 and ***P<0.001. GC, gastric cancer; ROS, reactive oxygen species.

treatment group was significantly lower than that in the control and single-drug groups (Fig. 4B), whereas the clonogenic ability was significantly reduced (Fig. 4C), and the mortality rate was significantly elevated (Fig. 4D). Additionally, western blot analysis revealed that the expression levels of the proapoptotic proteins BAX and cleaved caspase-3 were increased, whereas the expression of the antiapoptotic protein BCL-2 was decreased in the combination treatment group (Fig. 4E). These results indicated that Hesperadin enhances the antiproliferative effect of cisplatin, promotes apoptosis, and thereby potentiates the cytotoxic effect of cisplatin on GC cells.

Hesperadin enhances the sensitivity of GC cells to cisplatin via oxidative stress. Cisplatin exerts its anticancer effect mainly by binding to DNA to form cross-links and induce the production of ROS, thereby leading to apoptosis (4,5). The present study revealed that Hesperadin significantly inhibits GC cell proliferation and induces cell death by inducing ROS generation (Figs. 1C and 3). Therefore, it was next explored whether Hesperadin could increase the sensitivity of GC cells to cisplatin through oxidative stress. First, the fluorescence intensity in the Hesperadin-cisplatin combination treatment group was significantly greater than that in the single-drug treatment groups (Fig. 5A); the same results were obtained through quantitative flow cytometric analysis (Fig. 5B). Furthermore, it was found that both Hesperadin alone and cisplatin significantly reduced the MMP, whereas the combined treatment caused a further significant reduction in the MMP (Fig. 5C). Additionally, the fluorescence intensity of the DNA damage marker γ-H2AX was measured. The results revealed that γ-H2AX fluorescence intensity in the single-drug treatment groups (Hesperadin or cisplatin) was significantly higher than in the control group, whereas the combination treatment group demonstrated a further significant increase in γ-H2AX fluorescence intensity (Fig. 5D), indicating more extensive DNA damage following combination treatment. Collectively, these findings indicated that Hesperadin enhances the sensitivity of GC cells to cisplatin by promoting ROS generation, disrupting MMP, exacerbating DNA damage, and thereby facilitating cell death.

Hesperadin enhances the sensitivity of GC cells to cisplatin by activating NOX1-induced oxidative stress. To directly investigate whether the chemo-sensitizing effect of Hesperadin toward cisplatin was mediated through the NOX1/ROS axis, as suggested by our transcriptomic data, the upregulation of NOX1 expression was first confirmed. Through RT-qPCR analysis, it was found that NOX1 expression was significantly upregulated upon Hesperadin treatment in GC (Fig. 6A). In addition, western blot analysis confirmed that the Hesperadin alone, cisplatin alone, and combination treatments significantly increased the protein expression level of NOX1 in AGS cells. In HGC-27 cells, the increase in NOX1 protein following cisplatin treatment did not reach statistical significance, highlighting a cell-type-dependent difference in response. However, the combination treatment with Hesperadin robustly

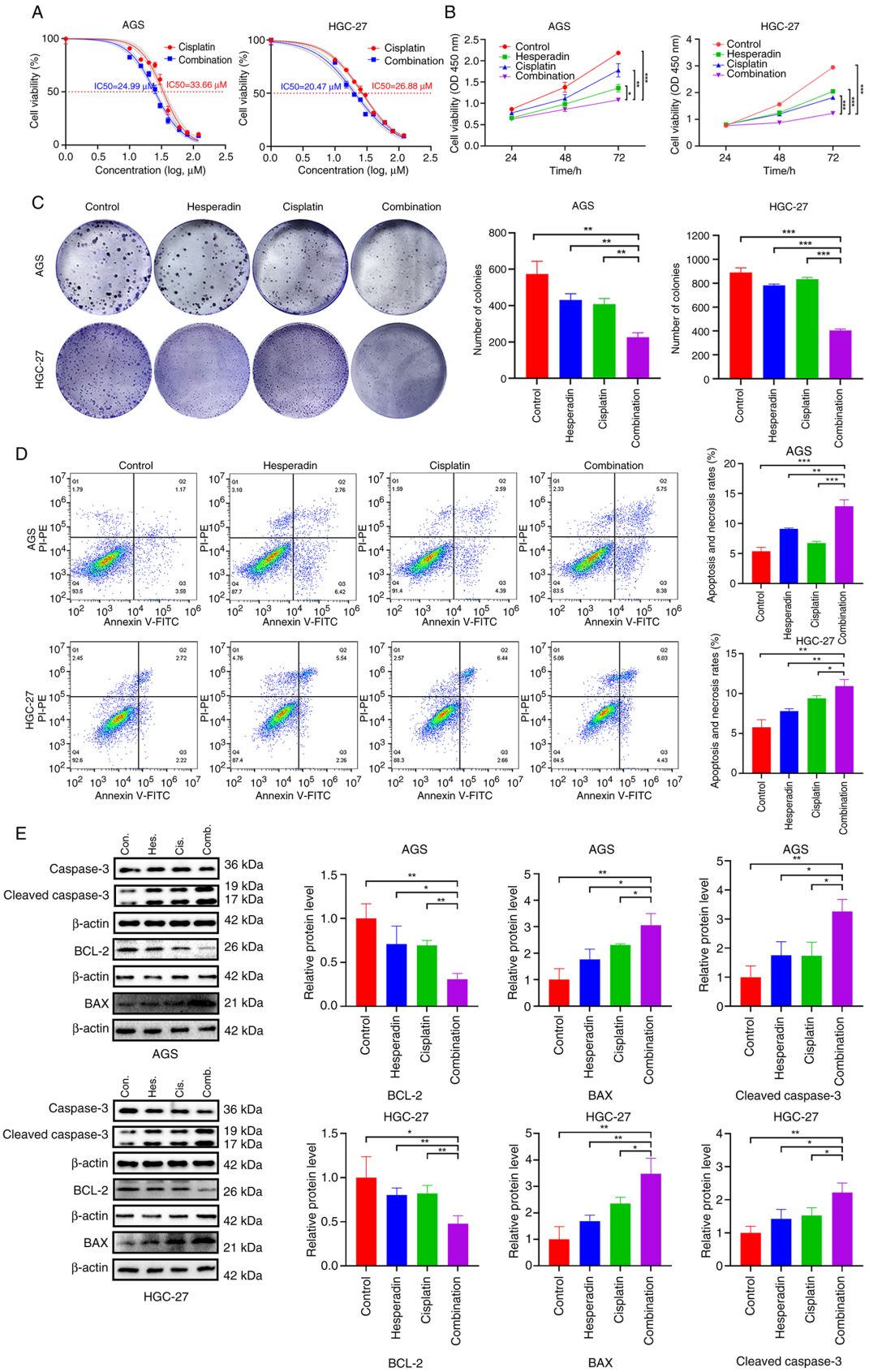

Figure 4. Hesperadin enhances the sensitivity of gastric cancer cells to cisplatin. (A) Changes in the IC_{50} of cisplatin in AGS and HGC-27 cells after 48 h of cotreatment with Hesperadin (10 nM) and various concentrations of cisplatin (0, 10, 15, 20, 25, 30, 40, 60, 80, or 120 nM). (B) Cell Counting Kit-8 assay for cell viability after 24, 48 and 72 h of cotreatment with Hesperadin and cisplatin. (C) Colony formation assay to assess the ability of cells to form colonies after 10 days of cotreatment. (D) Flow cytometric analysis showing cell mortality after cotreatment with Hesperadin and cisplatin. (E) Western blot analysis was used to evaluate the expression of apoptosis-related proteins (BCL-2, BAX and cleaved caspase-3). β-ACTIN was used as a loading control. Hesperadin concentrations were 20 nM for AGS cells and 16 nM for HGC-27 cells, whereas cisplatin concentrations were 10 μM for AGS cells and 8 μM for HGC-27 cells. Compared with all the other groups (Control, Hes. alone, Cis. alone); *P<0.05, **P<0.01 and ***P<0.001. Con., Control; Hes., Hesperadin; Cis., Cisplatin; Comb., Combination.

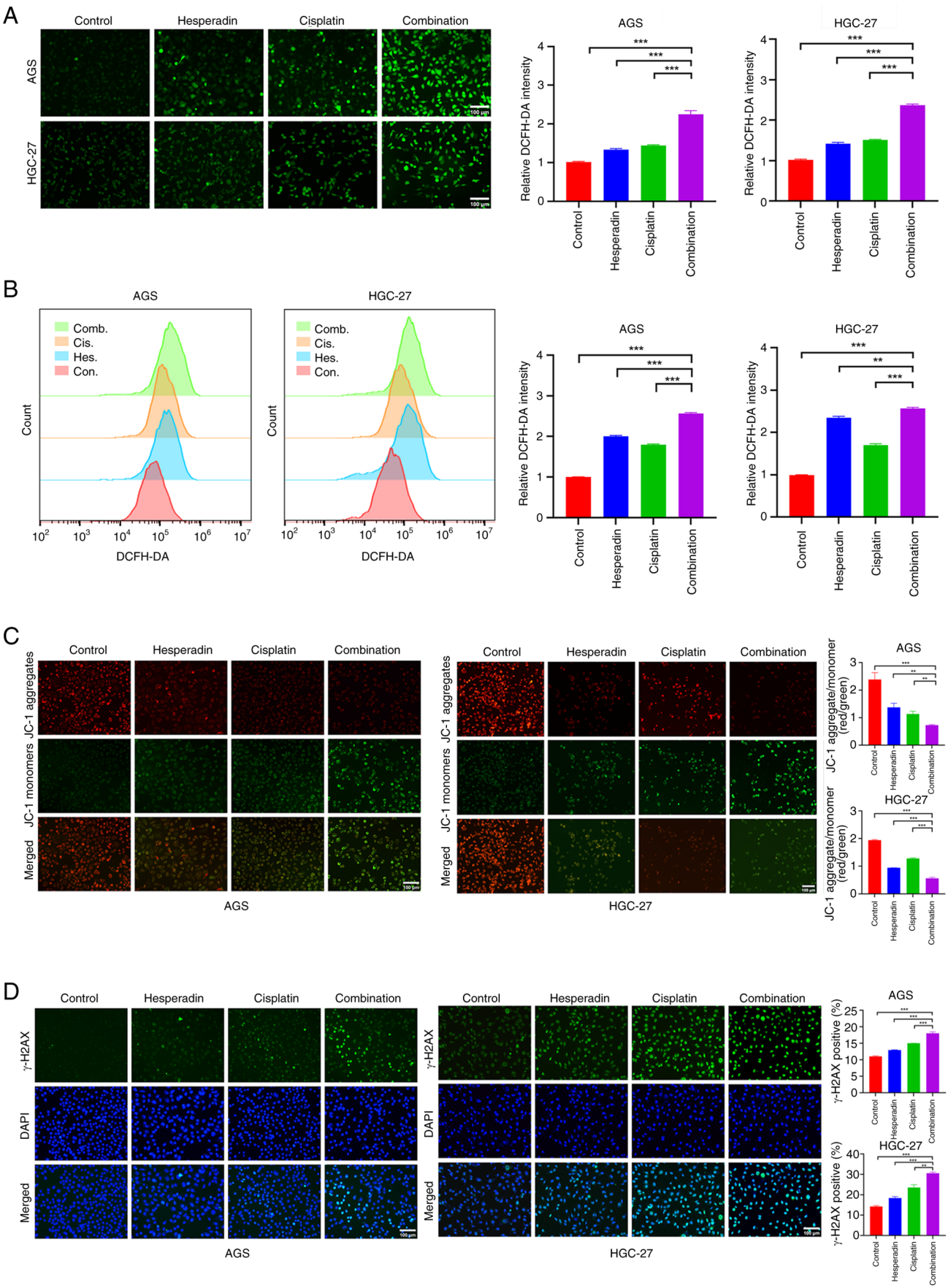

Figure 5. Hesperadin increases the sensitivity of gastric cancer cells to cisplatin via oxidative stress. (A) DCFH-DA fluorescence staining (green fluorescence represents ROS) showing changes in ROS levels following treatment with Hesperadin and cisplatin. (B) Quantification of ROS levels by flow cytometry. (C) JC-1 fluorescence staining was used to detect changes in the MMP. (D) γ-H2AX fluorescence staining was used to measure the level of DNA damage (blue: nuclei; green: γ-H2AX); (scale bar, 100 μm). Compared with all the other groups (Control, Hes. alone, Cis. alone); **P<0.01 and ***P<0.001. ROS, reactive oxygen species.

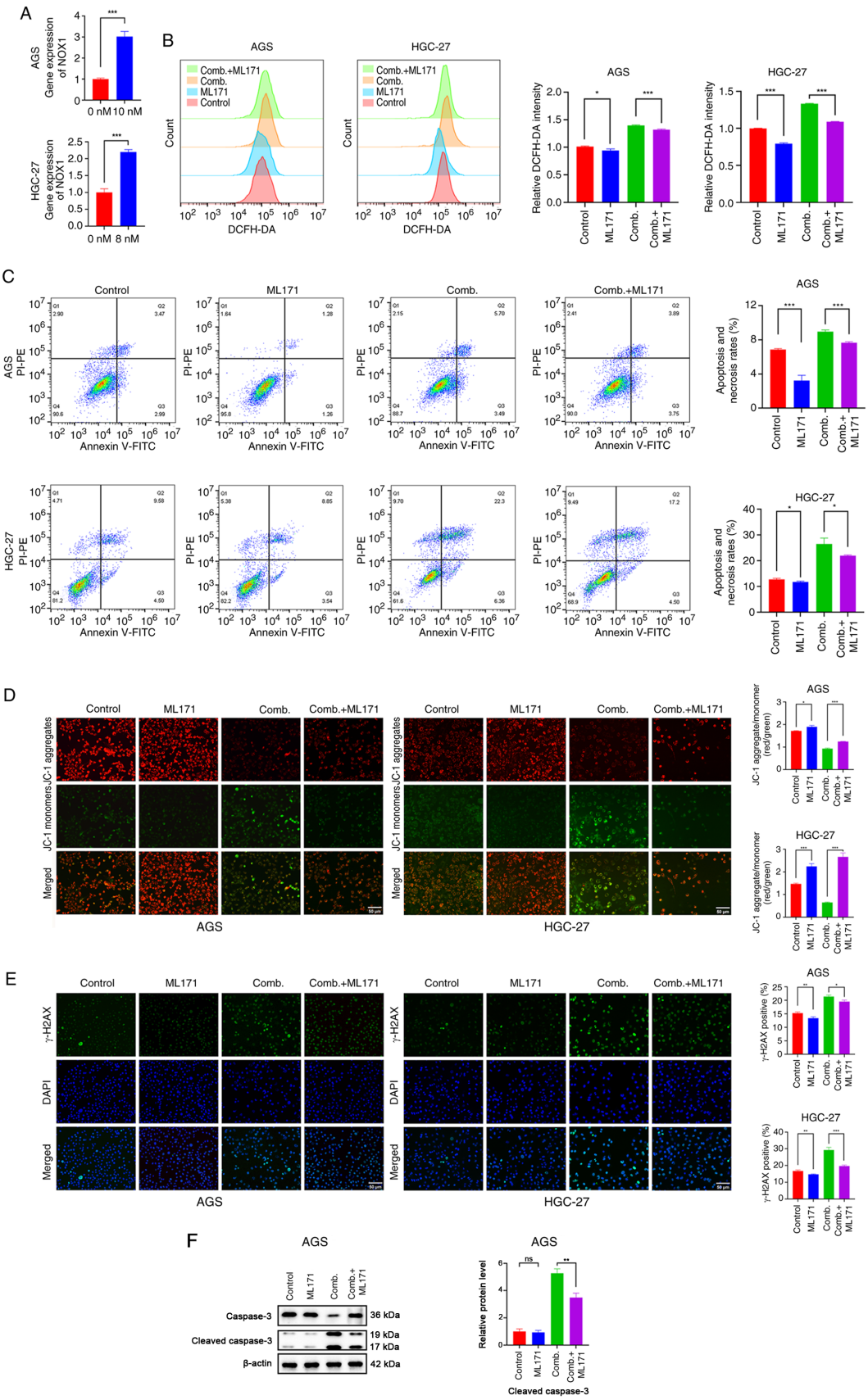

Figure 6. Hesperadin enhances the sensitivity of GC cells to cisplatin by activating NOX1-induced oxidative stress. (A) The mRNA expression level of NOX1 in GC cells after Hesperadin treatment, as determined by reverse transcription-quantitative PCR. (B-E) GC cells were pre-treated with or without the NOX1 inhibitor ML171 (0.2 μM) for 2 h, followed by combination treatment (Hesperadin + Cisplatin). The effects on (B) reactive oxygen species generation, (C) cell death, (D) MMP and (E) DNA damage were assessed using flow cytometry and immunofluorescence analysis (scale bar, 50 μm). (F) Western blot analysis of Cleaved Caspase-3 levels in AGS cells from the experiment shown in C. The blot confirms the induction of apoptosis by the combination treatment at the molecular level, corroborating the flow cytometry data. β-ACTIN was used as a loading control. Comb. + ML171 vs. Comb; *P<0.05, **P<0.01 and ***P<0.001. GC, gastric cancer; ns, not significant (P≥0.05).

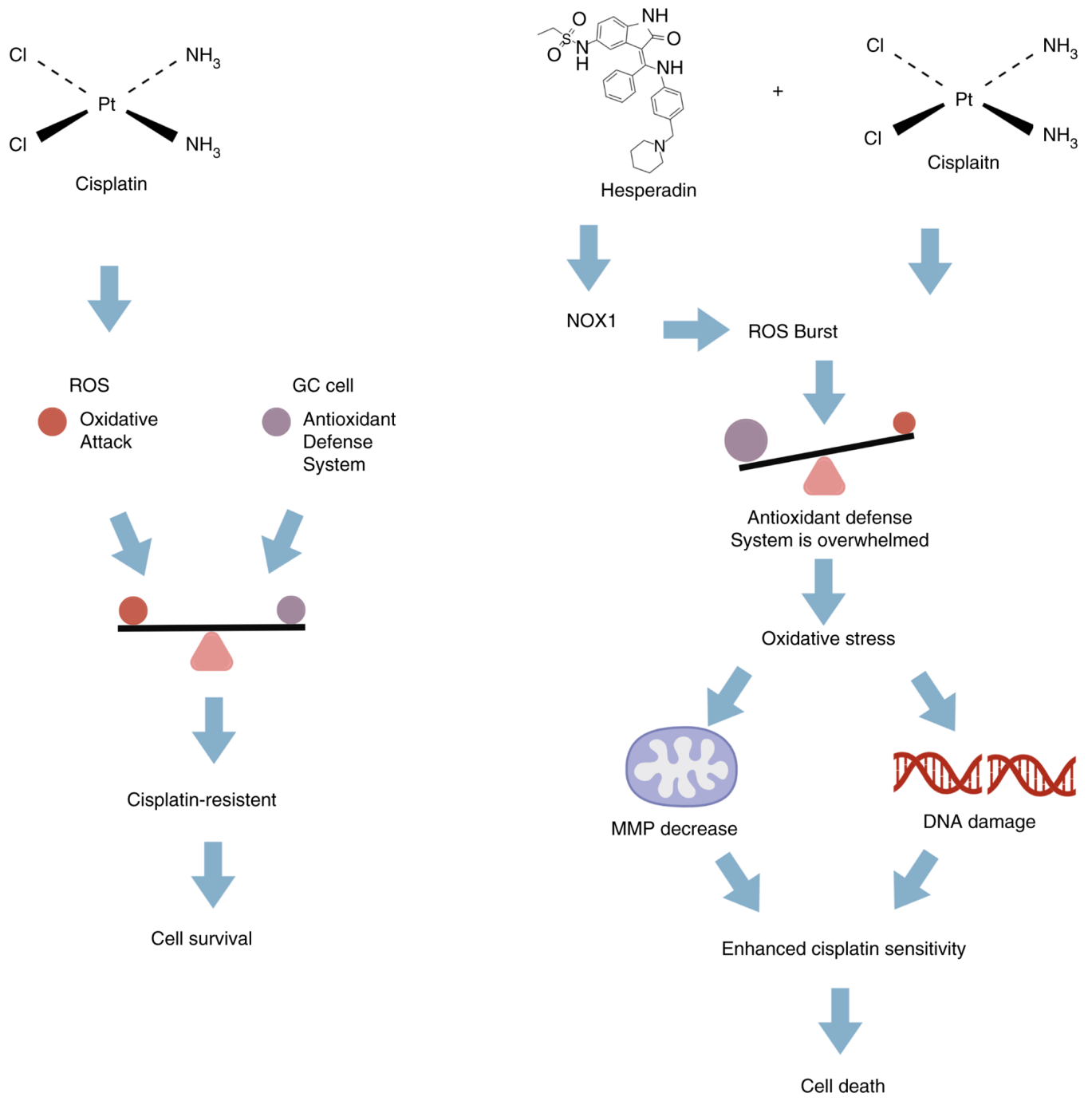

Figure 7. Schematic diagram demonstrating how hesperadin potentiates the chemosensitivity to cisplatin in GC cells via NOX1-mediated oxidative stress. The image was created with BioGDP.com (33). GC, gastric cancer; ROS, reactive oxygen species.

increased NOX1 levels in both cell lines (Fig. S1C), which was consistent with the observed transcriptional changes. To validate the functional role of NOX1, siRNA was subsequently used to knock down NOX1 expression in AGS and HGC-27 cells. Compared with si-NC transfection, NOX1-specific siRNA transfection significantly reduced NOX1 protein levels (Fig. S1A). ML171, a highly selective NOX1 inhibitor, was subsequently employed to evaluate the role of NOX1 in Hesperadin-induced oxidative stress and its impact on cisplatin sensitivity in GC cells. The results revealed that both ML171 treatment and NOX1 knockdown markedly attenuated the generation of ROS induced by the combination of cisplatin and Hesperadin (Figs. 6B and S1B). Furthermore, NOX1 inhibition rescued the cell death caused by the combined treatment (Fig. 6C). MMP analysis revealed that NOX1 inhibition partially reversed the MMP reduction induced by the combination treatment (Fig. 6D). Additionally, γ-H2AX immunofluorescence analysis revealed that NOX1 inhibition significantly attenuated DNA damage in the combination treatment group (Fig. 6E). To provide molecular substantiation for the flow cytometry results in AGS cells, western blot analysis for Cleaved Caspase-3 was performed using the same treatments. Consistent with the functional data, the combination treatment significantly increased the level of Cleaved

Caspase-3, which was significantly reversed by co-treatment with the NOX1 inhibitor ML171 (Fig. 6F). Collectively, these findings indicated that Hesperadin promotes ROS generation through NOX1-mediated oxidative stress in GC cells.

Discussion

Hesperadin was initially synthesized as a novel indolinone compound during anti-proliferative screening and was subsequently identified as a potent Aurora B kinase inhibitor that disrupts mitosis by impairing chromosome segregation and spindle assembly checkpoint function (23). Its mechanisms of action not only include G_2/M phase cell cycle arrest through Aurora B inhibition but also involve the induction of DNA damage, oxidative stress (ROS generation), endoplasmic reticulum stress, and mitochondrial dysfunction, ultimately promoting cancer apoptosis (16,24). Additionally, Hesperadin has been identified as a selective inhibitor of CaMKII-δ, suggesting potential cardioprotective effects (15). It also acts as a broad-spectrum anti-influenza agent effective against both influenza A and B viruses, including oseltamivir-resistant strains (25). However, its application and mechanism in the treatment of GC have not yet been extensively studied.

In the present study, it was confirmed that Hesperadin significantly inhibits GC cell proliferation and induces apoptosis while enhancing the chemosensitivity of GC cells to cisplatin. To elucidate the underlying mechanism, transcriptomic analysis and identified NOX1 was performed, a key member of the NADPH oxidase family, as an upstream regulator of Hesperadin's action. Combined treatment with Hesperadin and cisplatin significantly upregulated NOX1 expression. Importantly, inhibition of NOX1 substantially reversed the ROS generation and cytotoxic effects induced by the combination treatment. These results demonstrated that Hesperadin enhances cisplatin sensitivity in GC cells primarily through NOX1-mediated ROS overproduction. Notably, Hesperadin can modulate NOX1 expression, and cisplatin has also been shown to do so in other models. Research by Kim *et al* (26) in auditory cells showed that cisplatin upregulates NOX1 expression by inducing the release of pro-inflammatory cytokines (for example, TNF-α, IL-1β and IL-6) and activating the MAPK/ERK signaling pathway. However, the specific mechanism by which cisplatin regulates NOX1 in GC requires further investigation. On the other hand, as a dual inhibitor of Aurora B and CAMKII-δ, Hesperadin may influence ROS responses through multiple pathways. Aurora B, a key mitotic regulator, is involved in DNA damage response and cell survival under genotoxic stress. Its inhibition may compromise DNA repair fidelity, thereby amplifying cisplatin-induced DNA damage and ROS accumulation (27,28). Meanwhile, CAMKII-δ is known to participate in redox signaling and mitochondrial regulation in various cell types (29,30). Although its role in GC remains unclear, it was hypothesized that CAMKII-δ may similarly regulate NOX1 activity or mitochondrial ROS generation in GC cells. Elucidating the specific mechanisms and potential crosstalk between Hesperadin and cisplatin in regulating NOX1 will be a focus of our future research. However, the present study has certain limitations. First, the present findings require further validation in *in vivo* animal models to confirm the therapeutic efficacy and safety profile of the Hesperadin and cisplatin combination. Second, it is important to note that our mechanistic focus on NOX1 and oxidative stress was influenced by prior literature (31,32) and the established role of ROS in Hesperadin's action in other cancers (16). While the present RNA-seq data supported this focus (Fig. 2C and D), this targeted approach may have introduced a selection bias, potentially overlooking other DEGs with higher fold changes or unknown functions in GC (Table SI) that could also contribute to the observed phenotype. Moreover, the precise molecular mechanisms by which Hesperadin regulates NOX1 expression and mediates oxidative stress warrant deeper investigation. Specifically, the upstream regulatory mechanisms (for example, how Hesperadin activates NOX1 transcription/translation through specific signaling pathways) and the downstream effector protein interaction network following NOX1-mediated ROS generation remain insufficiently elucidated. Research indicates that the regulation of NOX1 by cisplatin in auditory cells is associated with inflammatory signaling, whereas the mechanism by which Hesperadin modulates NOX1 in GC cells remains unclear. Although the present RNA-seq analysis implicated potential involvement of pathways such as p53, NF-κB and PI3K-Akt (Fig. 2D), these preliminary findings await future experimental validation to define their precise roles in this regulatory axis.

In summary, the present study demonstrated that Hesperadin sensitizes GC cells to cisplatin by triggering NOX1-mediated oxidative stress and mitochondrial dysfunction-induced apoptosis (Fig. 7). Additionally, the current findings indicated that the combination of Hesperadin and cisplatin represents a promising therapeutic strategy for the treatment of GC.

Acknowledgements

Not applicable.

Funding

The present study was supported by the Natural Science Foundation of Bengbu Medical College (grant no. 2022byfy002), the Graduate Research Innovation Program of Bengbu Medical College (grant no. Byycx24005), the University Synergy Innovation Program of Anhui (grant no. GXXT-2022-065) and the Natural Science Program of Bengbu Medical University (grant no. 2023byzd030).

Availability of data and materials

The data generated in the present study may be found in the NCBI Sequence Read Archive under accession numbers SRR35296175, SRR35296174, SRR35296173, SRR35296169, SRR35296168 and SRR35296167 or at the following URL: https://www.ncbi.nlm.nih.gov/sra/?term=SRR35296175; https://www.ncbi.nlm.nih.gov/sra/?term=SRR35296174; https://www.ncbi.nlm.nih.gov/sra/?term=SRR35296173; https://www.ncbi.nlm.nih.gov/sra/?term=SRR35296169; https://www.ncbi.nlm.nih.gov/sra/?term=SRR35296168; https://www.ncbi.nlm.nih.gov/sra/?term=SRR35296167. The data generated in the present study may be requested from the corresponding author.

Authors' contributions

WJZ, HZW and YLZ conceptualized the study. ZLJ, QYL, WJZ and DW analyzed and curated data. ZLJ, QYL, JYC and WJZ conducted investigation. JYC designed and established the experimental methodology. WJZ, ZLJ, QYL and DW wrote the original draft. WJZ and HZW revised the manuscript. All authors wrote, reviewed and edited the manuscript. All authors read and approved the final version of the manuscript. WJZ and HZW confirm the authenticity of all the raw data.

Ethics approval and consent to participate

Not applicable.

Patient consent for publication

Not applicable.

Competing interests

The authors declare that they have no competing interests.

References

1. Bray F, Laversanne M, Sung H, Ferlay J, Siegel RL, Soerjomataram I and Jemal A: Global cancer statistics 2022: GLOBOCAN estimates of incidence and mortality worldwide for 36 cancers in 185 countries. CA Cancer J Clin 74: 229-263, 2024.
2. Digklia A and Wagner AD: Advanced gastric cancer: Current treatment landscape and future perspectives. World J Gastroenterol 22: 2403-2414, 2016.
3. Lei ZN, Teng QX, Tian Q, Chen W, Xie Y, Wu K, Zeng Q, Zeng L, Pan Y, Chen ZS and He Y: Signaling pathways and therapeutic interventions in gastric cancer. Signal Transduct Target Ther 7: 358, 2022.
4. Huang R and Zhou PK: DNA damage repair: Historical perspectives, mechanistic pathways and clinical translation for targeted cancer therapy. Signal Transduct Target Ther 6: 254, 2021.
5. Peña Q, Wang A, Zaremba O, Shi Y, Scheeren HW, Metselaar JM, Kiessling F, Pallares RM, Wuttke S and Lammers T: Metallodrugs in cancer nanomedicine. Chem Soc Rev 51: 2544-2582, 2022.
6. Ruhlmann CH, Iversen TZ, Okera M, Muhic A, Kristensen G, Feyer P, Hansen O and Herrstedt J: Multinational study exploring patients' perceptions of side-effects induced by chemoradiotherapy. Radiother Oncol 117: 333-337, 2015.
7. Shahid M, Subhan F, Ahmad N and Sewell RDE: The flavonoid 6-methoxyflavone allays cisplatin-induced neuropathic allodynia and hypoalgesia. Biomed Pharmacother 95: 1725-1733, 2017.
8. Yu C, Dong H, Wang Q, Bai J, Li YN, Zhao JJ and Li JZ: Danshensu attenuates cisplatin-induced nephrotoxicity through activation of Nrf2 pathway and inhibition of NF-κB. Biomed Pharmacother 142: 111995, 2021.
9. Wang H, Zhang Z, Wei X and Dai R: Small-molecule inhibitor of Bcl-2 (TW-37) suppresses growth and enhances cisplatin-induced apoptosis in ovarian cancer cells. J Ovarian Res 8: 3, 2015.
10. Shi S, Bai X, Ji Q, Wan H, An H, Kang X and Guo S: Molecular mechanism of ion channel protein TMEM16A regulated by natural product of narirutin for lung cancer adjuvant treatment. Int J Biol Macromol 223: 1145-1157, 2022.
11. Bai X, Liu Y, Cao Y, Ma Z, Chen Y and Guo S: Exploring the potential of cryptochlorogenic acid as a dietary adjuvant for multi-target combined lung cancer treatment. Phytomedicine 132: 155907, 2024.
12. Morahan BJ, Abrie C, Al-Hasani K, Batty MB, Corey V, Cowell AN, Niemand J, Winzeler EA, Birkholtz LM, Doerig C and Garcia-Bustos JF: Human Aurora kinase inhibitor hesperadin reveals epistatic interaction between Plasmodium falciparum PfArk1 and PfNek1 kinases. Commun Biol 3: 701, 2020.
13. Wu X, Wu J, Hu W, Wang Q, Liu H, Chu Z, Lv K and Xu Y: MST4 kinase inhibitor Hesperadin attenuates autophagy and behavioral disorder via the MST4/AKT pathway in intracerebral hemorrhage mice. Behav Neurol 2020: 2476861, 2020.
14. Chhajer R, Bhattacharyya A and Ali N: Cell death in Leishmania donovani promastigotes in response to Mammalian Aurora kinase B inhibitor-Hesperadin. Biomed Pharmacother 177: 116960, 2024.
15. Zhang J, Liang R, Wang K, Zhang W, Zhang M, Jin L, Xie P, Zheng W, Shang H, Hu Q, *et al*: Novel CaMKII-δ inhibitor Hesperadin exerts dual functions to ameliorate cardiac ischemia/reperfusion injury and inhibit tumor growth. Circulation 145: 1154-1168, 2022.
16. Zhang Y, Wu J, Fu Y, Yu R, Su H, Zheng Q, Wu H, Zhou S, Wang K, Zhao J, *et al*: Hesperadin suppresses pancreatic cancer through ATF4/GADD45A axis at nanomolar concentrations. Oncogene 41: 3394-3408, 2022.
17. Livak KJ and Schmittgen TD: Analysis of relative gene expression data using real-time quantitative PCR and the 2(-Delta Delta C(T)) method. Methods 25: 402-408, 2001.
18. Carneiro BA and El-Deiry WS: Targeting apoptosis in cancer therapy. Nat Rev Clin Oncol 17: 395-417, 2020.
19. Li J, Jia YC, Ding YX, Bai J, Cao F and Li F: The crosstalk between ferroptosis and mitochondrial dynamic regulatory networks. Int J Biol Sci 19: 2756-2771, 2023.
20. To TL, Cuadros AM, Shah H, Hung WHW, Li Y, Kim SH, Rubin DHF, Boe RH, Rath S, Eaton JK, *et al*: A compendium of genetic modifiers of mitochondrial dysfunction reveals intra-organelle buffering. Cell 179: 1222-1238.e17, 2019.
21. Wagner AD, Syn NL, Moehler M, Grothe W, Yong WP, Tai BC, Ho J and Unverzagt S: Chemotherapy for advanced gastric cancer. Cochrane Database Syst Rev 8: CD004064, 2017.
22. Al-Batran SE, Homann N, Pauligk C, Goetze TO, Meiler J, Kasper S, Kopp HG, Mayer F, Haag GM, Luley K, *et al*: Perioperative chemotherapy with fluorouracil plus leucovorin, oxaliplatin, and docetaxel versus fluorouracil or capecitabine plus cisplatin and epirubicin for locally advanced, resectable gastric or gastro-oesophageal junction adenocarcinoma (FLOT4): A randomised, phase 2/3 trial. Lancet 393: 1948-1957, 2019.
23. Hauf S, Cole RW, LaTerra S, Zimmer C, Schnapp G, Walter R, Heckel A, van Meel J, Rieder CL and Peters JM: The small molecule Hesperadin reveals a role for Aurora B in correcting kinetochore-microtubule attachment and in maintaining the spindle assembly checkpoint. J Cell Biol 161: 281-294, 2003.
24. Ladygina NG, Latsis RV and Yen T: Effect of the pharmacological agent hesperadin on breast and prostate tumor cultured cells. Biomed Khim 51: 170-176, 2005 (In Russian).
25. Hu Y, Zhang J, Musharrafieh R, Hau R, Ma C and Wang J: Chemical genomics approach leads to the identification of Hesperadin, an Aurora B kinase inhibitor, as a broad-spectrum influenza antiviral. Int J Mol Sci 18: 1929, 2017.
26. Kim HJ, Lee JH, Kim SJ, Oh GS, Moon HD, Kwon KB, Park C, Park BH, Lee HK, Chung SY, *et al*: Roles of NADPH oxidases in cisplatin-induced reactive oxygen species generation and ototoxicity. J Neurosci 30: 3933-3946, 2010.
27. Chen TM, Huang CM, Setiawan SA, Hsieh MS, Sheen CC and Yeh CT: KDM5D histone demethylase identifies platinum-tolerant head and neck cancer cells vulnerable to mitotic catastrophe. Int J Mol Sci 24: 5310, 2023.
28. Han X, Zhang JJ, Han ZQ, Zhang HB and Wang ZA: Let-7b attenuates cisplatin resistance and tumor growth in gastric cancer by targeting AURKB. Cancer Gene Ther 25: 300-308, 2018.
29. Erickson JR, Joiner ML, Guan X, Kutschke W, Yang J, Oddis CV, Bartlett RK, Lowe JS, O'Donnell SE, Aykin-Burns N, *et al*: A dynamic pathway for calcium-independent activation of CaMKII by methionine oxidation. Cell 133: 462-474, 2008.
30. Anderson ME, Brown JH and Bers DM: CaMKII in myocardial hypertrophy and heart failure. J Mol Cell Cardiol 51: 468-473, 2011.
31. Zhang Z, Zhao X, Gao M, Xu L, Qi Y, Wang J and Yin L: Dioscin alleviates myocardial infarction injury via regulating BMP4/NOX1-mediated oxidative stress and inflammation. Phytomedicine 103: 154222, 2022.
32. Drummond GR, Selemidis S, Griendling KK and Sobey CG: Combating oxidative stress in vascular disease: NADPH oxidases as therapeutic targets. Nat Rev Drug Discov 10: 453-471, 2011.
33. Jiang S, Li H, Zhang L, Mu W, Zhang Y, Chen T, Wu J, Tang H, Zheng S, Liu Y, *et al*: Generic diagramming platform (GDP): A comprehensive database of high-quality biomedical graphics. Nucleic Acids Res 53 (D1): D1670-D1676, 2025.